Simulations of the turbulent channel flow at $Re_\tau = 180$ with projection-based finite element variational multiscale methods

Volker John[*,†] and Michael Roland

FR 6.1—Mathematik, Universität des Saarlandes, Postfach 15 11 50, Saarbrücken 66041, Germany

SUMMARY

Projection-based variational multiscale (VMS) methods, within the framework of an inf–sup stable second order finite element method for the Navier–Stokes equations, are studied in simulations of the turbulent channel flow problem at $Re_\tau = 180$. For comparison, the Smagorinsky large eddy simulation (LES) model with van Driest damping is included into the study. The simulations are performed on very coarse grids. The VMS methods give often considerably better results. For second order statistics, however, the differences to the reference values are sometimes rather large. The dependency of the results on parameters in the eddy viscosity model is much weaker for the VMS methods than for the Smagorinsky LES model with van Driest damping. It is shown that one uniform refinement of the coarse grids allows an underresolved direct numerical simulations (DNS). Copyright © 2007 John Wiley & Sons, Ltd.

1. INTRODUCTION

Turbulent incompressible flows occur in many processes in nature and industry. The accurate simulation of such flows is, however, still a major challenge. Due to the limited resolution of discretizations for the underlying incompressible Navier–Stokes equations, it is not possible to resolve (and thus to simulate) all scales of a turbulent flow [1]. The unresolved scales are important for the turbulent character of the flow and their influence onto the resolved scales has to be taken into account by means of a turbulence model. There are many approaches for turbulence modelling, for instance, k–ε models, classical large eddy simulation (LES) models, Navier–Stokes-α-models,

---

[*]Correspondence to: Volker John, FR 6.1—Mathematik, Universität des Saarlandes, Postfach 15 11 50, Saarbrücken 66041, Germany.
[†]E-mail: john@math.uni-sb.de

WILEY
InterScience®
DISCOVER SOMETHING GREAT

approximate deconvolution models or variational multiscale (VMS) models. We will study in this paper a class of VMS models at the benchmark problem of the turbulent channel flow at $Re_\tau = 180$ and compare the results with a classical LES model.

Classical LES methods are currently one of the most popular approaches for the simulation of incompressible turbulent flows. A classical LES method starts by decomposing the flow field into large (resolved) scales and small (unresolved) scales. A characteristic feature of these methods is the definition of the large scales by an average in space, using a convolution with an appropriate filter function or a so-called differential filter (which is an approximation of a convolution operator). The aim of classical LES methods consists in simulating accurately only the large scales of the flow field, thereby modelling the influence of the small scales onto the large ones with the help of a turbulence model, see the monographs [2–4] for details. Widely used classical LES models are Smagorinsky-type models [5], for instance, the dynamic Smagorinsky model by Germano *et al.* [6] and Lilly [7].

A more recently proposed alternative approach for incompressible turbulent flow simulations are VMS methods. Their development is based on general ideas for the simulation of multiscale phenomena from [8, 9]. The first presentation of a VMS approach for turbulent flows can be found in [10]. The basis of a VMS method for incompressible flows is a decomposition of the flow field into three scales; resolved large scales; resolved small scales; and unresolved small scales [11]. Similar to classical LES models, the goal of a VMS method consists in simulating all resolved scales, or at least the large scales, accurately. However, an essential difference to classical LES methods consists in the way of defining the scales. In VMS methods, the scales are defined by projections into appropriate subspaces of the space in which the variational formulation of the problem is given. Another essential difference consists in the way of applying the turbulence model which models the influence of the unresolved scales. Whereas in the classical LES approach, the turbulence model is applied directly to all resolved scales, a VMS method applies it directly only to the resolved small scales. By the coupling of scales, there is an indirect influence of the turbulence model to the resolved large scales as well. A VMS method tries to restrict in this way the direct application of the turbulence model to the scales where it is needed. This is similar to the goal of the dynamic Smagorinsky LES model by Germano and Lilly, which dynamically adjusts a factor in the Smagorinsky model to control the influence of this model in the simulations. For an introduction to VMS models and their relations and differences to classical LES models, we refer to the survey papers [12, 13].

Since presenting the idea of using the VMS approach for turbulent flow simulations in [10], a number of numerical studies have been published applying methods of this kind. Among the first ones are [14, 15] using Fourier spectral methods for the simulation of homogeneous isotropic turbulence and turbulent channel flows (at $Re_\tau \in \{180, 395\}$), respectively. The study [15] was later complemented by [16] for $Re_\tau = 590$ and by [17], which studies the dependency of the results on the separation of scales in terms of wave numbers. In [18], the so-called planar VMS method was applied to turbulent channel flow simulations at $Re_\tau \in \{180, 590\}$. In the planar VMS method, a Fourier–Galerkin method was used in streamwise and spanwise direction, like in the Fourier spectral method, whereas a finite volume discretization was applied in wall normal direction. The scale separation of the VMS approach has been performed only in planes orthogonal to the wall normal direction. The same authors also developed the local VMS method which is based on a discontinuous Galerkin discretization. Turbulent channel flow simulations with this method can be found, for instance, in [19] ($Re_\tau = 100$) and [20] ($Re_\tau \in \{100, 395\}$). In [21, 22], a VMS method for a second order, energy conserving finite volume method is

presented. This method defines the large scales by restricting the discrete functions to the next coarser grid and prolongating the coarse functions appropriately back to the fine grid. Turbulent channel flow computations are presented for $Re_\tau \in \{180, 590\}$. For further applications of the VMS idea in the simulation of turbulent flows, we refer to [23, 24].

Numerical studies of VMS methods which include a comparison with the classical dynamic Smagorinsky LES model, for instance, in [14, 15, 18, 22, 24], show that the VMS methods give in general better results.

The parameters of a VMS method in the context of finite element methods (FEMs) are finite element spaces which define a scale separation and the turbulence model acting directly on the resolved small scales. Concerning the turbulence model, almost all simulations which can be found in the literature so far use Smagorinsky-type models, often the standard Smagorinsky model [5], see Section 3 for details. With respect to the spaces for the scale separation, there are principally different realizations. The first one utilizes separate finite element spaces for the large scales and for the resolved small scales. It requires the solution of equations for the resolved small scales. For the large scales, standard finite element spaces are used. On the one hand, the finite element spaces for the resolved small scales have to have in some sense a better resolution than the finite element spaces for the large scales. On the other hand, the solution of the equations for the resolved small scales should be not too expensive. For these reasons, it is proposed to use bubble functions for the resolved small scales, which leads to a localization of the small-scale problems. This so-called bubble VMS method has been studied, for instance, in [25, 26]. A second realization of a VMS method uses a standard finite element space for all resolved scales and an additional finite element space for the large space, see [27] and Section 3 for detailed descriptions. This so-called projection-based VMS method will be used in the numerical simulations presented in this paper. The VMS method of [21, 22], which is based on a finite volume method, has a similar spirit like the two-level version of the projection-based finite element VMS method, which was shortly mentioned in [27] and presented in detail (for convection–diffusion equations) in [28]. For a detailed description of bubble and projection-based VMS methods, we refer to [29]. A third way of achieving a scale separation in finite element VMS methods was used in [30]. This method exploits the hierarchy of hierarchical basis functions for velocity and pressure: ansatz functions up to a certain polynomial degree represent the large scales and the ansatz functions of higher degree the resolved small scales.

A natural framework of VMS methods are finite element methods since they are based on a variational formulation of the underlying equation. Finite element methods have so far been widely used in the simulation of laminar flows. It has been shown that in particular higher order finite element methods (at least second order velocity and first order pressure) lead to quite accurate results, for instance, in [31, 32] for flows around a cylinder. Thus, it seems naturally to apply finite element discretizations also in the turbulent regime. However, finite element methods have been used far less than Fourier spectral methods, finite difference methods (FDMs) or finite volume methods (FVMs) for the simulation of turbulent flows. This might have several reasons. The other methods are traditionally popular in the engineering community and most of the simulations have been performed by scientist having an engineering background. Another reason might be the higher complexity of implementing finite element methods. There are only very few examples for the application of higher order finite element methods in turbulent flow simulations, like [19, 20, 27]. In fact, to our best knowledge, the current paper presents the first study of a turbulent channel flow which uses inf–sup stable second order finite elements for the velocity and first order finite elements for the pressure. It will be shown that for the turbulent channel flow with $Re_\tau = 180$ good

results for the mean velocity profile are obtained even on very coarse grids with roughly 17 000 and 29 000 degrees of freedom (d.o.f.). The results for second order statistics are less accurate, however, in view of the coarseness of the grids often still satisfactory.

For the coarse grids, the application of a turbulence model becomes necessary. A question of interest to explore is up to which fineness of the meshes turbulence models are needed. It will be shown that refining these coarse grids once and obtaining thus 116 000 and 232 000 d.o.f., respectively, the application of the Galerkin finite element discretization is already possible, which can be interpreted as an underresolved direct numerical simulation (DNS) or as a Monotone integrated LES (MILES) approach.

The paper is organized as follows. In Section 2, the turbulent channel flow problem, the discretizations, the grids and the computation of the statistics of interest are explained in detail. The computations on the coarse grids are presented in Section 3. This section contains also a detailed description of the used turbulence models. Section 4 briefly presents the results for the Galerkin finite element method on the finer grids. The results of the computational studies are summarized in Section 5.

2. SET-UP OF THE NUMERICAL SIMULATIONS

2.1. The turbulent channel flow at $Re_\tau = 180$

The turbulent channel flow is governed by the (non-dimensionalized) incompressible Navier–Stokes equations

$$\frac{\partial \mathbf{u}}{\partial t} - 2\nabla \cdot (Re_\tau^{-1} \mathbb{D}(\mathbf{u})) + (\mathbf{u} \cdot \nabla)\mathbf{u} + \nabla p = \mathbf{f} \quad \text{in } (0, T] \times \Omega$$

$$\nabla \cdot \mathbf{u} = 0 \quad \text{in } [0, T] \times \Omega \tag{1}$$

where

$$\Omega = (-2\pi, 2\pi) \times (0, 2H) \times (-\tfrac{2}{3}\pi, \tfrac{2}{3}\pi)$$

$\mathbb{D}(\mathbf{u}) = (\nabla \mathbf{u} + \nabla \mathbf{u}^{\mathrm{T}})/2$ being the velocity deformation tensor, $H = 1$ being the channel half width and $Re_\tau = 180$ being the Reynolds number based on the channel half width, the kinematic viscosity v of the fluid and the shear or friction velocity u_τ, see [1] for the definition of u_τ. The dimensions of the channel are standard ones for this Reynolds number [1, 33]. There are periodic conditions in the streamwise x- and the spanwise z-direction for the velocity $\mathbf{u}$ on the boundary and no-slip conditions for the solid walls at $y = 0$ and 2.

The definition of an initial condition in our simulations is based on the discrete mean velocity profile $U_{\mathrm{mean}}^{\mathrm{DNS}}(y)$ from the data file `chan180.means` provided in [33]. The discrete mean velocity profile is interpolated linearly, giving $U_{\mathrm{mean}}^{\mathrm{DNS,lin}}(y)$, and noise is added in the same form as in [22]

$$\mathbf{u}_1(0; x, y, z) = U_{\mathrm{mean}}^{\mathrm{DNS,lin}}(y) + 0.1\, U_{\mathrm{bulk}}\psi$$

$$\mathbf{u}_2(0; x, y, z) = 0.1\, U_{\mathrm{bulk}}\psi \tag{2}$$

$$\mathbf{u}_3(0; x, y, z) = 0.1\, U_{\mathrm{bulk}}\psi$$

The bulk velocity is computed by

$$U_{\text{bulk}} = \frac{1}{H} \int_0^H U_{\text{mean}}^{\text{DNS,spline}}(y) \, \mathrm{d}y = 15.6803 \tag{3}$$

where $U_{\text{mean}}^{\text{DNS,spline}}(y)$ is a cubic spline interpolation of $U_{\text{mean}}^{\text{DNS}}(y)$. The noise is given by a random function ψ with values in $[-1, 1]$. This function, in $C++$-notation

$$\psi = \frac{2\,\text{rand}()}{\text{RAND\_MAX}()} - 1 \in [-1, 1]$$

is called for each degree of freedom and each component of the velocity. Altogether, the initial velocity field (2) is obtained by disturbing the linearly interpolated mean velocity profile $U_{\text{mean}}^{\text{DNS,lin}}(y)$ by a random velocity fluctuation of up to 10% of the bulk velocity U_{bulk} either in negative or positive direction.

Since the flow is incompressible, the bulk velocity should be constant during the simulations. However, finite element functions are in general only discretely divergence free. Thus, a finite element discretization will not lead automatically to a conservation of the bulk velocity. We account for the difference of the computed bulk velocity and (3) by a dynamic adjustment of the right-hand side of the Navier–Stokes equations. The flow is driven by a pressure gradient. Let $U_{\text{bulk,sim}}(t_n)$ be the bulk velocity of the computed solution at time t_n. Then, we define the right-hand side of the Navier–Stokes equations (1) at t_{n+1} by

$$\mathbf{f} = \begin{pmatrix} 1 \\ 0 \\ 0 \end{pmatrix} + \frac{1}{\Delta t_n} \begin{pmatrix} U_{\text{bulk}} - U_{\text{bulk,sim}}(t_n) \\ 0 \\ 0 \end{pmatrix} \tag{4}$$

where Δt_n is the length of the time step. That means, if $U_{\text{bulk,sim}}(t_n) < U_{\text{bulk}}$, the flow will be accelerated which leads to an increase in the bulk velocity of the computed solution. In the case $U_{\text{bulk,sim}}(t_n) > U_{\text{bulk}}$, the mean speed of the flow will be slowed down below 1 and $U_{\text{bulk,sim}}$ becomes smaller.

If the dynamic adjustment of the driving force (4) were not applied, we could observe increase as well as decrease in the bulk velocity of the computed solution, depending on the turbulence model. Using (4), the bulk velocity still showed some oscillations but it stayed always close (differences in general far less than 1%) to the value given in (3).

2.2. The discretization

Here, we will restrict ourselves to the description of the discretization of the Navier–Stokes equations (1). The treatment of additional terms in the turbulence models is presented in Section 3.

Standard notations for Lebesgue and Sobolev spaces are used. Let $(\cdot, \cdot)$ denote the inner product in $(L^2(\Omega))^d$, $d \geqslant 1$. The space V is defined by

$$V = \{\mathbf{v} \in (H^1(\Omega))^3 : \mathbf{v} = \mathbf{0} \text{ on } y = 0 \text{ and } y = 2\}$$

and the space $Q = L_0^2(\Omega)$, the space of all functions from $L^2(\Omega)$ with integral mean value zero.

Our approach of discretizing (1) is as follows:

1. Discretize (1) by the Crank–Nicolson scheme in time. This gives for the discrete time t_n the system

$$\mathbf{u}_n + \tfrac{1}{2}\Delta t_n[-2\nabla \cdot (Re_\tau^{-1}\mathbb{D}(\mathbf{u}_n)) + (\mathbf{u}_n \cdot \nabla)\mathbf{u}_n] + \Delta t_n \nabla p_n$$
$$= \mathbf{u}_{n-1} + \tfrac{1}{2}\Delta t_n\mathbf{f}_n + \tfrac{1}{2}\Delta t_n\mathbf{f}_{n-1} - \tfrac{1}{2}\Delta t_n[-2\nabla \cdot (Re_\tau^{-1}\mathbb{D}(\mathbf{u}_{n-1})) \qquad (5)$$
$$+ (\mathbf{u}_{n-1} \cdot \nabla)\mathbf{u}_{n-1}]$$

$$\nabla \cdot \mathbf{u}_n = 0$$

where Δt_n is the length of the time step from t_{n-1} to t_n and $\mathbf{u}_n = \mathbf{u}(t_n)$, etc. Note that there is an inconsistency in the temporal discretization of the pressure, see [3] for a discussion of this issue.

2. Transform (5) into a variational form: find $(\mathbf{u}_n, p_n) \in V \times Q$ such that

$$(\mathbf{u}_n, \mathbf{v}) + \tfrac{1}{2}\Delta t_n[(2Re_\tau^{-1}\mathbb{D}(\mathbf{u}_n), \mathbb{D}(\mathbf{v})) + ((\mathbf{u}_n \cdot \nabla)\mathbf{u}_n, \mathbf{v})] - \Delta t_n(p_n, \nabla \cdot \mathbf{v})$$
$$= (\mathbf{u}_{n-1}, \mathbf{v}) + \tfrac{1}{2}\Delta t_n(\mathbf{f}_n, \mathbf{v}) + \tfrac{1}{2}\Delta t_n(\mathbf{f}_{n-1}, \mathbf{v}) - \tfrac{1}{2}\Delta t_n[(Re_\tau^{-1}\mathbb{D}(\mathbf{u}_{n-1}), \mathbb{D}(\mathbf{v})) \qquad (6)$$
$$+((\mathbf{u}_{n-1} \cdot \nabla)\mathbf{u}_{n-1}, \mathbf{v})]$$

$$(\nabla \cdot \mathbf{u}_n, q) = 0$$

for all $(\mathbf{v}, q) \in V \times Q$.

3. Solve (6) by a fixed point iteration: given $\mathbf{u}_n^{(0)} = \mathbf{u}_{n-1}$, solve the linear system (Oseen system): find $(\mathbf{u}_n^{(k)}, p_n^{(k)}) \in V \times Q$

$$(\mathbf{u}_n^{(k)}, \mathbf{v}) + \tfrac{1}{2}\Delta t_n[(2Re_\tau^{-1}\mathbb{D}(\mathbf{u}_n^{(k)}), \mathbb{D}(\mathbf{v})) + ((\mathbf{u}_n^{(k-1)} \cdot \nabla)\mathbf{u}_n^{(k)}, \mathbf{v})] - \Delta t_n(p_n^{(k)}, \nabla \cdot \mathbf{v})$$
$$= (\mathbf{u}_{n-1}, \mathbf{v}) + \tfrac{1}{2}\Delta t_n(\mathbf{f}_n, \mathbf{v}) + \tfrac{1}{2}\Delta t_n(\mathbf{f}_{n-1}, \mathbf{v}) - \tfrac{1}{2}\Delta t_n[(Re_\tau^{-1}\mathbb{D}(\mathbf{u}_{n-1}), \mathbb{D}(\mathbf{v})) \qquad (7)$$
$$+ ((\mathbf{u}_{n-1} \cdot \nabla)\mathbf{u}_{n-1}, \mathbf{v})]$$

$$(\nabla \cdot \mathbf{u}_n, q) = 0$$

for all $(\mathbf{v}, q) \in V \times Q$, $k = 0, 1, \ldots$

4. Discretize (7) by the Q_2/P_1^{disc} finite element method, i.e. the velocity is approximated by a piecewise triquadratic continuous function and the pressure by a piecewise linear discontinuous function.

We would like to present some motivations for choosing this way of discretizing (1). The Crank–Nicolson scheme is well known to be an accurate and efficient temporal discretization of the incompressible Navier–Stokes equations, see [34–36]. Likewise, the Q_2/P_1^{disc} finite element discretization is known to be among the best performing finite elements for incompressible flows, see in particular [37] and our own experiences in [3, 31, 35, 38]. Note that finite element methods for the physically correct deformation tensor formulation are considerably more expensive than for the gradient formulation $(Re_\tau\nabla\mathbf{u}, \nabla\mathbf{v})$, cf. the discussion of this topic in [3]. The linearization by a fixed point iteration was shown to be more efficient than using a Newton method in [35].
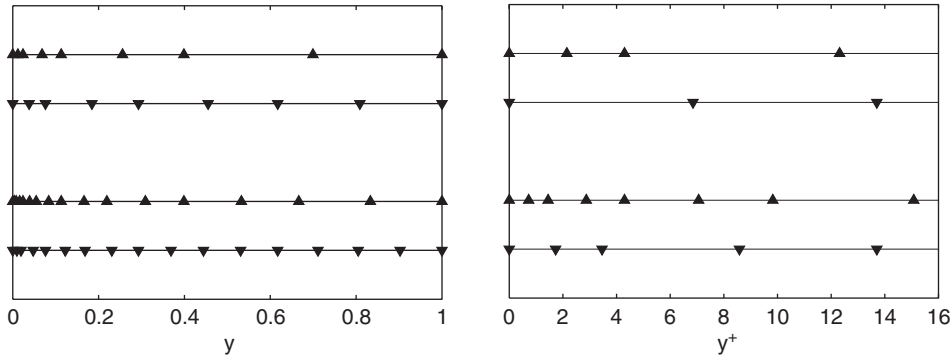
Figure 1. Distributions of the degrees of freedom in wall normal direction, level 2, left: $y \in [0, 1]$, right: zoom near the wall; from top to bottom: Grid 0, $l0 = 2$; Grid 1, $l0 = 2$; Grid 0, $l0 = 4$; Grid 1, $l0 = 4$.

The Crank–Nicolson scheme was applied with an equidistant time step of $\Delta t = 0.002$ ($\Delta t^+ := u_\tau$ $Re_\tau \Delta t = 0.36$, where the value $u_\tau = 1$ of the statistically steady state has been used). This is considerably smaller than the Kolmogorov time scale and it fits into the range of the time step proposed in [39].

Simulations on two different grids were performed in our numerical studies. The grids were obtained by uniform refinement from a coarsest grid (level 0) using a subdivision of the hexahedral mesh cells into eight smaller mesh cells. In the periodic directions (x and z), the grid spacings are uniform. The coarsest grid in streamwise and spanwise direction is a 2×2 uniform grid. In the wall normal direction, one has to use non-uniform grids which become finer towards the walls. We will study two different grids, which describe the distribution of the grid points in wall normal direction as follows:

Grid 0:

$$y_i = 1 + \frac{\tanh(\gamma(2i/N_y - 1))}{\tanh(\gamma)}, \quad i = 0, \ldots, N_y$$

with $\gamma = 2.75$, see [39]; also [19, 40] for turbulent channel flows with different Reynolds numbers where also different stretching factors γ have been used;

Grid 1:

$$y_i = 1 - \cos\left(\frac{i\pi}{N_y}\right), \quad i = 0, \ldots, N_y$$

see [21, 22].

Here, N_y is the number of mesh cell layers in wall normal direction. Consequently, the number of grid points in y-direction, including the points on the boundaries, is $N_y + 1$. Concerning the coarsest grid, we will study grids with two layers (denoted by $l0 = 2$) and with four layers ($l0 = 4$). After each uniform refinement step, the points of the new grid are translated into wall normal direction such that the prescribed distribution is attained. Since the velocity is approximated with the Q_2 finite element, there are $2N_y + 1$ layers of d.o.f. in y direction, including the boundary. Note that due to the definition of the Q_2 finite element, the layers of d.o.f. between the grid points do not obey the prescribed distribution but they are located half way between the grid points, see Figure 1.

Table I. Information on the grids used in the computations.

Level	$l0$	Cells	N_y	Vel. d.o.f.	Press. d.o.f.	Grid 0, $y^+_{\min}$	Grid 1, $y^+_{\min}$
2	2	512	8	15 104	2048	2.1480	6.8508
2	4	1024	16	25 344	4096	0.7244	1.7293
3	2	4096	16	101 376	16 384	0.7244	1.7293
3	4	8112	32	199 680	32 768	0.3012	0.4386

Let $y^+ = Re_\tau y = 180y$, $y \in [0, 1]$, be the distance from the wall measured in wall units (or viscous lengths). The distributions of the d.o.f. in wall normal direction for our numerical simulations on level 2 are presented in Figure 1. It can be seen that the hyperbolic tangent function (Grid 0) places the d.o.f. with a higher density closer to the wall than the cosine function (Grid 1).

Information concerning the grids are given in Table I: the number of mesh cells, the number of d.o.f., the distance of the d.o.f. next to the walls $y^+_{\min}$ and the number N_y of mesh cell layers are given. It is hard to compare the fineness of the grids to resolutions of completely different discretizations like Fourier–Galerkin methods. Information on the number of d.o.f. are given for the discontinuous Galerkin methods used in [19]. Level 2 of our grids has in both cases fewer d.o.f. than the grids in [19], whereas the number of d.o.f. on level 3 has the same order of magnitude like in [19].

2.3. Statistics of interest

We will use the reference data for the turbulent channel flow at $Re_\tau = 180$ which can be found in the data files belonging to the DNS simulations from [33].

Let $\langle \cdot \rangle_s$ denote the spatial averaging over the directions of homogeneity. Since uniform grids are used in streamwise and spanwise direction, the spatial averaging can be performed by the arithmetic mean. Let $\mathbf{u}^h(t, x, y, z)$ be the computed flow field. Then, the spatial mean velocity at time t_n in the plane $y = \text{const.}$ is computed by

$$\mathbf{U}^h(t_n, y) := \langle \mathbf{u}^h(t_n, x, y, z) \rangle_s = \frac{1}{N_x N_z} \sum_{i=1}^{N_x} \sum_{j=1}^{N_z} \mathbf{u}^h(t_n, x_i, y, z_j)$$

where $N_x (N_z)$ is the number of d.o.f. in the streamwise (spanwise) direction in the plane $y = \text{const.}$ This is done for all planes $y = \text{const.}$ which contain velocity d.o.f. in wall normal direction, see Figure 1.

The average in time will be denoted by $\langle \cdot \rangle_t$. Since equidistant time steps will be used in the computations, the arithmetic mean is again applied. Thus, the mean velocity profile is given by

$$\mathbf{U}^h_{\text{mean}}(y) := \langle \langle \mathbf{u}^h(t_n, x, y, z) \rangle_s \rangle_t = \frac{1}{N_t + 1} \sum_{n=0}^{N_t} \mathbf{U}^h(t_n, y)$$

We will present results for the first component $U^h_{\text{mean}}(y)$ of $\mathbf{U}^h_{\text{mean}}(y)$.

The simulated friction velocity u^h_τ is defined as the average of the computed friction velocities at both walls, where the friction velocity at each wall is approximated by a one-sided difference

$$u^h_\tau := \frac{1}{2} \left(\frac{U^h_{\text{mean}}(y^+_{\min})}{y^+_{\min}} - \frac{U^h_{\text{mean}}(2 - y^+_{\min})}{2 - y^+_{\min}} \right)$$

Second order statistics of interest in turbulent channel flows are the off-diagonal Reynolds stresses and the root mean square (rms) turbulence intensities. Unfortunately, the definition of the averaged Reynolds stresses does not seem to be unique in the literature. Denoting by u the streamwise velocity component and by v the wall normal component, the Reynolds stress $\mathbb{R}_{12} = \mathbb{R}_{uv} = \mathbb{R}_{xy}$ can be defined by

$$\mathbb{R}_{12} := \langle \langle uv \rangle_s \rangle_t - \langle \langle u \rangle_s \rangle_t \langle \langle v \rangle_s \rangle_t \tag{8}$$

or alternatively by

$$\tilde{\mathbb{R}}_{12} := \langle \langle uv \rangle_s \rangle_t - \langle \langle u \rangle_s \langle v \rangle_s \rangle_t = \langle \langle uv \rangle_s - \langle u \rangle_s \langle v \rangle_s \rangle_t \tag{9}$$

The form (8) can be found, for instance, in [41] for theoretical considerations and in [21, 22, 42] for computations. Formula (9) was used, for instance, in [15], where in particular

$$\langle \langle (u^h - \langle u^h \rangle_s)^2 \rangle_s \rangle_t^{1/2} = \langle \langle u^h u^h - 2\langle u^h \rangle_s u^h + \langle u^h \rangle_s \langle u^h \rangle_s \rangle_s \rangle_t^{1/2}$$

$$= \langle \langle u^h u^h \rangle_s - 2\langle u^h \rangle_s \langle u^h \rangle_s + \langle u^h \rangle_s \langle u^h \rangle_s \rangle_t^{1/2}$$

$$= (\tilde{\mathbb{R}}_{11}^h)^{1/2}$$

was considered. The definitions (8) and (9) are in general not identical. Spatial and temporal averaging can be interchanged in (8) whereas this is not possible in (9). It is not clear which form, (8) or (9), was used to compute the reference data in [33].

The computation of the statistics in the numerical studies presented below follows [41]. The off-diagonal Reynolds stresses of the DNS from [33] can be approximated by

$$\mathbb{R}_{ij}^{\text{DNS}} \approx \mathbb{R}_{ij}^h + \langle \langle \mathbb{A}_{ij}^h \rangle_s \rangle_t, \quad i, j = 1, 2, 3, \ i \neq j$$

where the approach (8) is used to compute $\mathbb{R}_{ij}^h$ and $\mathbb{A}_{ij}^h$ stands for the modelled subgrid scale stresses. A normalization with $(u_\tau^h)^2$ was used to compute the off-diagonal Reynolds stresses presented below

$$\mathbb{R}_{ij}^{h,*} := \frac{\mathbb{R}_{ij}^h + \langle \langle \mathbb{A}_{ij}^h \rangle_s \rangle_t}{(u_\tau^h)^2}, \quad i, j = 1, 2, 3, \ i \neq j \tag{10}$$

Concerning the diagonal stresses, their deviation from isotropy can be approximated by [41]

$$\mathbb{R}_{ii}^{\text{DNS}} - \frac{1}{3} \sum_{j=1}^{3} \mathbb{R}_{jj}^{\text{DNS}} \approx \mathbb{R}_{ii}^h + \langle \langle \mathbb{A}_{ii}^h \rangle_s \rangle_t - \frac{1}{3} \sum_{j=1}^{3} (\mathbb{R}_{jj}^h + \langle \langle \mathbb{A}_{jj}^h \rangle_s \rangle_t), \quad i = 1, 2, 3$$

Then, the rms turbulence intensities given for the simulations below are computed with a normalization with u_τ^h, for instance

$$u_{\text{rms}}^{h,*} := \frac{\left| \mathbb{R}_{11}^h + \langle \langle \mathbb{A}_{11}^h \rangle_s \rangle_t - \frac{1}{3} \sum_{j=1}^{3} (\mathbb{R}_{jj}^h + \langle \langle \mathbb{A}_{jj}^h \rangle_s \rangle_t) \right|^{1/2}}{u_\tau^h} \tag{11}$$

The form of the subgrid scale model $\mathbb{A}^h$ for the different models used in the computations, together with remarks for evaluating $\mathbb{A}^h$, is given in Section 3.

Let $\mathbb{R}_{ii}^{\mathrm{MKM}}$ denote the reference data of [33]. We compare the rms turbulence intensities, for instance, $u_{\mathrm{rms}}^{h,*}$, to

$$|\mathbb{R}_{11}^{\mathrm{MKM}} - \tfrac{1}{3}(\mathbb{R}_{11}^{\mathrm{MKM}} + \mathbb{R}_{22}^{\mathrm{MKM}} + \mathbb{R}_{33}^{\mathrm{MKM}})|^{1/2}$$

This approach follows [42]. Note that other comparisons can be found in the literature as well. For instance, in [15], the term $\langle\langle(u^h - \langle u^h\rangle_s)^2\rangle_s\rangle_t^{1/2}$ (plus influence of the turbulence model) is compared to $(\mathbb{R}_{11}^{\mathrm{MKM}})^{1/2}$.

Since the turbulent channel flow is statistically symmetric at $y = 1$, only the averaged values on half the channel are given below. These are computed by averaging the values obtained on both halves of the channel.

Starting with the initial condition (2), the turbulent channel flows were simulated with each method in the time interval $[0, 20]\,\mathrm{s}$ ($t^+ \in [0, 3600]$) to obtain a fully developed flow field which can be considered to be independent of the initial condition. We checked with other initial conditions (perturbed laminar flow profile) that the initial simulation time of 20 s was sufficient for achieving this goal. The mean velocity profiles were almost indistinguishable. The differences in the second order statistics were somewhat larger, however, neither the form of the curves, nor the magnitude of the values changed considerably. With the results at $t = 20\,\mathrm{s}$, the simulations were started anew for computing the time averages. The length of the time interval for computing the time averages was also 20 s.

The simulations were performed with the code *MooNMD* [43].

3. SIMULATIONS ON COARSE GRIDS WITH THE APPLICATION OF TURBULENCE MODELS

3.1. The turbulence models

In this section, the simulation of the turbulent channel flow at $Re_\tau = 180$ is considered on grids which are too coarse to allow the application of the Galerkin finite element method. The coarse grids described in Section 2 are refined twice to obtain these grids (level 2). The corresponding number of d.o.f. are given in Table I. The Galerkin finite element method blows up in final times on these grids. Thus, the application of a turbulence model becomes necessary. The following turbulence models are studied:

- the Smagorinsky LES model [5] with van Driest damping [44] (SvD), see also [1];
- the fully implicit projection-based VMS method with piecewise constant large-scale tensors (VMS P0), see [27];
- the fully implicit projection-based VMS method with discontinuous piecewise linear tensors (VMS P1), see [27].

It was shown in [21, 22] that on grids which allow the application of a Galerkin method (underresolved or coarse DNS), this method outperforms in general the methods with turbulence models. Thus, it is important to use grids which are sufficiently coarse to make the use of turbulence models meaningful.

The traditional Smagorinsky LES model introduces the additional term

$$(v_T \mathbb{D}(\mathbf{u}^h), \mathbb{D}(\mathbf{v}^h)), \quad v_T = C_s \delta_K^2 \|\mathbb{D}(\mathbf{u}^h)\|_F \tag{12}$$

into the Galerkin finite element method of the Navier–Stokes equations. In (12), C_s is a user-chosen constant, K denotes a mesh cell, δ_K is a parameter explained below and $\|\cdot\|_F$ is the Frobenius norm of a tensor. Usually, $\delta_K = ch_K$ is chosen where $c \in [1, 2]$ depends on the discretization (order of the finite element method, for Q_2, we use $c = 1$) and h_K is a measure of the cell width. The grids we are using consist of anisotropic mesh cells near the wall. The possible measures range from the shortest edge to the diameter of the mesh cells. Which is an appropriate one will be studied below, see Section 3.2.

Another characteristic feature of the Smagorinsky LES model is the production of too much energy dissipation near the walls. This issue will be addressed by the so-called van Driest damping, i.e. the introduction of a damping factor in the viscous sublayer region ($y^+ < 5$). Instead of the turbulent viscosity (12)

$$v_T = C_s \delta_K^2 \|\mathbb{D}(\mathbf{u}^h)\|_F \left(1 - \exp\left(\frac{-y^+}{A}\right)\right)^2, \quad y^+ < 5 \tag{13}$$

is used with $A = 26$ and the same constant C_s as in (12). The terms of the Smagorinsky model with van Driest damping (12), (13) were treated implicitly in our computations. The model of the subgrid-scale stresses, which is needed to compute the Reynolds stresses (10) and the rms turbulence intensities (11), has the form $\mathbb{A}^h = -v_T \mathbb{D}(\mathbf{u}^h)$.

The projection-based VMS method has the following form (continuous in time): find $\mathbf{u}^h:[0, T] \to V^h$, $p^h:(0, T] \to Q^h$ and $\mathbb{G}^H:[0, T] \to L^H$ satisfying

$$\left(\frac{\partial \mathbf{u}^h}{\partial t}, \mathbf{v}^h\right) + (2Re_\tau^{-1} \mathbb{D}(\mathbf{u}^h), \mathbb{D}(\mathbf{v}^h)) + ((\mathbf{u}^h \cdot \nabla)\mathbf{u}^h, \mathbf{v}^h) - (p^h, \nabla \cdot \mathbf{v}^h)$$

$$+ (v_T(\mathbb{D}(\mathbf{u}^h) - \mathbb{G}^H), \mathbb{D}(\mathbf{v}^h)) = (\mathbf{f}, \mathbf{v}^h) \quad \text{for all } \mathbf{v}^h \in V^h \tag{14}$$

$$(q^h, \nabla \cdot \mathbf{u}^h) = 0 \quad \text{for all } q^h \in Q^h$$

$$(\mathbb{D}(\mathbf{u}^h) - \mathbb{G}^H, \mathbb{L}^H) = 0 \quad \text{for all } \mathbb{L}^H \in L^H$$

Here, $V^h \times Q^h$ is a standard, inf–sup stable pair of finite element spaces, in our simulations $V^h = Q_2$, $Q^h = P_1^{\text{disc}}$. The tensor-valued space L^H represents the large scales of the velocity deformation tensor. They are defined in the third equation of (14) by an L^2-projection. The choice of L^H controls the scale separation: the larger L^H becomes, the smaller becomes the part of the resolved small scales among all resolved scales. Since higher order finite elements were used for velocity and pressure, L^H can be defined on the same grid as $V^h \times Q^h$ with low order polynomials. We used in the simulations $L^H = P_0$ (piecewise constant tensors) and $L^H = P_1^{\text{disc}}$ (piecewise linear but discontinuous tensors). The resulting methods will be called VMS P0 and VMS P1, respectively.

In comparison to the variational form of the Navier–Stokes equations, there is one additional term in the momentum equation of (14), the most right one on the left-hand side. The difference $\mathbb{D}(\mathbf{u}^h) - \mathbb{G}^H$ represents small scales since $\mathbb{G}^H$ are large scales of $\mathbb{D}(\mathbf{u}^h)$. Thus, this term adds the additional turbulent viscosity v_T to the small scales of the flow field. This is exactly one of

the basic ideas of VMS methods. For the turbulent viscosity ν_T, we use the Smagorinsky model given in (12).

Of course, the van Driest damping could have been used easily for the VMS methods. However, in our opinion, a potential advantage of the VMS approach is that simple models for the influence of the unresolved scales can be applied since these models act directly only on a part of the resolved scales and the importance of the model is reduced in this way. A constant Smagorinsky model was used in the first numerical simulations of turbulent flows with VMS methods [14, 15] and a dynamic model, for instance, in [45] (without comparison to the constant Smagorinsky model) and in [17]. In [17], it was shown that the constant Smagorinsky model within the VMS methods led to highly accurate results for appropriate scale separations (in terms of wave numbers of a Fourier spectral method) but the dynamic model was less sensitive to the chosen scale partition. Both models within a two-level VMS method based on a second order finite volume method were compared in turbulent channel flow problems in [22]. It turned out that the use of the constant coefficient Smagorinsky model (without van Driest damping) led to better results than the dynamic model with even less computational effort. Similar observations are reported for turbulent flow simulations in a diffuser [46]. Moreover, for a VMS method based on a finite volume discretization applied to compressible flows, [24], it was found that the dynamic computation of the Smagorinsky parameter does not improve the results obtained by considering a constant parameter. In view of these experiences, the use of a dynamic model in the VMS methods seems not to be promising at the moment, at least not for second order discretizations.

The additional term in the momentum equation in (14) is treated implicitly. For details of the algorithm, we refer to [27]. For computing the Reynolds stresses (10) and the rms turbulence intensities (11), the model of the subgrid-scale stresses has the form $\mathbb{A}^h = -\nu_T(\mathbb{D}(\mathbf{u}^h) - \mathbb{G}^H)$ for the projection-based VMS method.

The choice of the constant C_s is the main issue in Smagorinsky-type models. The traditional value for turbulent channel flows is $C_s = 0.01$ [47]. However, it is known, [48], that a good value depends on the actual type of the mesh, the refinement level of the mesh and most probably also on the underlying discretization. The numerical studies in [48] show that even the dynamic Smagorinsky model often does not give good values for C_s (which is for this model a function in space and time). To study the influence of the value of C_s for the different models, besides the traditional value, we will present also results for $C_s \in \{0.001, 0.005\}$.

The quantities (10) and (11) were computed in all positions where the velocity possesses d.o.f. These d.o.f. are located in particular at faces of the mesh cells. However, $\mathbb{D}(\mathbf{u}^h)$ and $\mathbb{G}^H$ are discontinuous finite element functions. For computing $\mathbb{A}^h$, these functions are mapped to continuous functions by computing a local weighted average. Let (x, y, z) be the position of a velocity degree of freedom and ω be the union of all mesh cells where this degree of freedom belongs to. Then

$$\tilde{\mathbb{D}}(\mathbf{u}^h)(x, y, z) := \sum_{K \in \omega} \frac{1}{|K|} \mathbb{D}(\mathbf{u}^h)|_K(x, y, z)$$

where $|K|$ is the volume of the mesh cell K and $|_K$ denotes the restriction of the finite element function to K. An analogous formula is used for $\mathbb{G}^H$. In this way, one obtains the continuous Q_2 finite element functions $\tilde{\mathbb{D}}(\mathbf{u}^h)$ and $\tilde{\mathbb{G}}^H$ and these functions are used to compute $\mathbb{A}^h$ in the SvD and in the VMS methods. Note that the issue of smoothing the derivatives of the velocity arises from the low regularity of standard finite element functions.
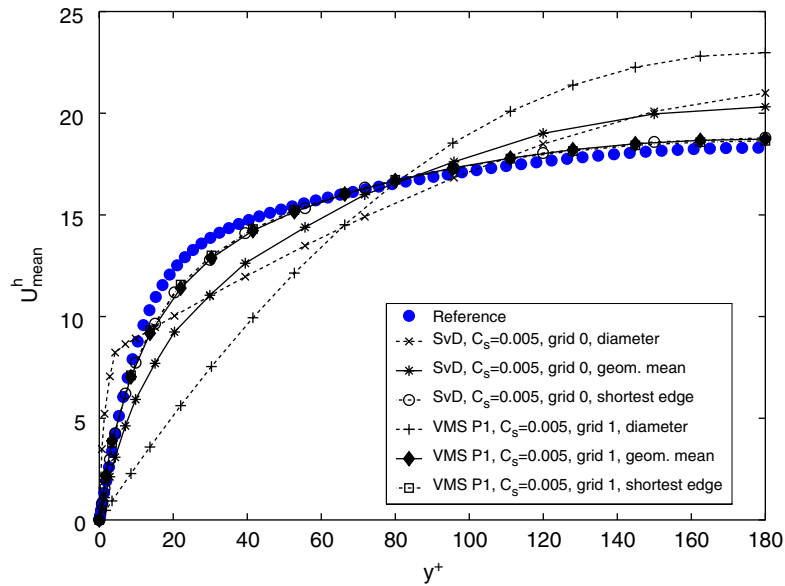
Figure 2. Mean velocity profile obtained with h_K being the diameter of the mesh cells, $h_K = \sqrt[3]{h_x h_y h_z}$ and h_K being the shortest edge of the mesh cells.

3.2. Simulations with different measures for the width of a mesh cell

The parameter δ_K of the Smagorinsky LES model with van Driest damping (12)–(13) as well as of the projection-based VMS methods (14) involves a measure h_K of the size of the mesh cells. Figure 2 presents some representative results which are obtained with:

- h_K being the diameter of the mesh cells (longest distance between two points of the mesh cells);
- $h_K = \sqrt[3]{h_x h_y h_z}$, where h_x, h_y, h_z are the sizes of the edges of the mesh cells in the coordinate directions (geometric mean);
- h_K being the shortest edge.

The use of the geometric mean can be found in the literature [18, 21, 22, 42]. Figure 2 presents mean velocity profiles U_{mean}^h for the SvD on Grid 1, level 2, $l0 = 4$, $C_s = 0.005$ and the projection-based VMS P1 on Grid 0, level 2, $l0 = 4$, $C_s = 0.005$. The results where h_K is chosen to be the shortest edge are the best ones for both models. The curves for the VMS method with h_K being the geometric mean and h_K being the shortest edge are almost indistinguishable. For the SvD, the result becomes considerably worse for h_K being the geometric mean. If h_K is chosen to be the diameter, very bad results are obtained for both methods.

In the remainder of the paper, we will only present results which are obtained with h_K chosen to be the shortest edge of the mesh cells.

3.3. Simulations on grids with an initial subdivision into two layers

The results of the simulations on the grids where the initial grid consists of two mesh cell layers, $l0 = 2$, and which were refined twice are presented in Figures 3–7.
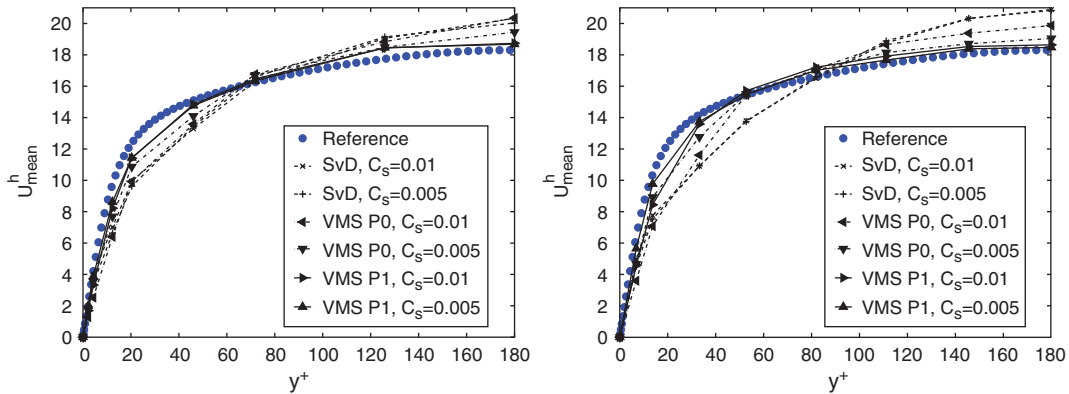
Figure 3. Simulations on the grids with an initial subdivision in y-direction into two layers, level 2, computed mean velocity profiles, Grid 0 (left) and Grid 1 (right).
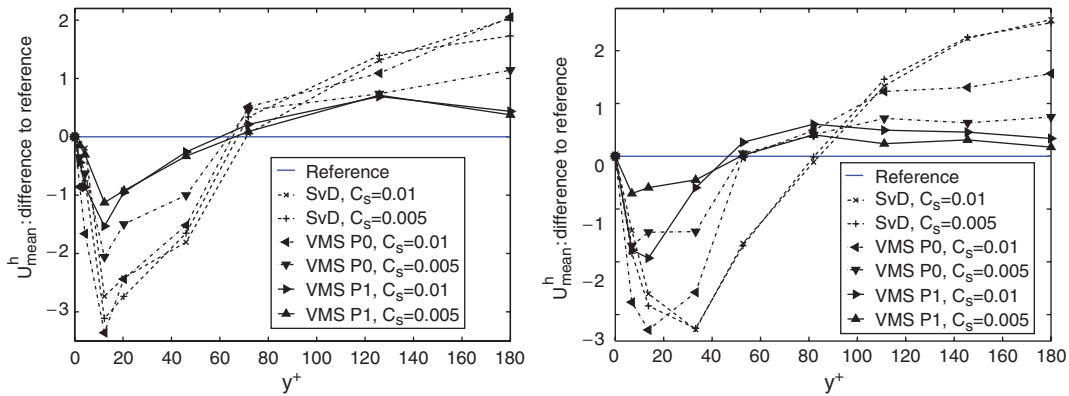

Figure 4. Simulations on the grids with an initial subdivision in y-direction into two layers, level 2, differences to the reference mean velocity profile, Grid 0 (left) and Grid 1 (right).

The results for the streamwise mean velocity, Figures 3 and 4, are much better for the VMS methods, in particular for VMS P1, than for the SvD method. The best results have been obtained with VMS P1 and $C_s = 0.005$. Even on these very coarse grids, the mean velocity profile is rather close to the reference one. Among the VMS methods, only the results for VMS P0 with $C_s = 0.01$ are unsatisfactory. The mean velocity profiles computed with the SvD method tend towards the profile for a laminar flow.

The computed rms turbulent intensities $u_{\mathrm{rms}}^{h,*}$ are shown in Figure 5. We present only results for $u_{\mathrm{rms}}^{h,*}$ since the evaluation of the results for $v_{\mathrm{rms}}^{h,*}$ and $w_{\mathrm{rms}}^{h,*}$ would be very similar. The curves obtained with the VMS methods (save VMS P0, $C_s = 0.01$, Grid 1) have in principle the correct form but the values are overpredicted. This overprediction is somewhat smaller on Grid 0. The curves computed with the SvD method do not possess the correct form. In addition, there is a heavy underprediction of the values at the wall for $C_s = 0.01$.
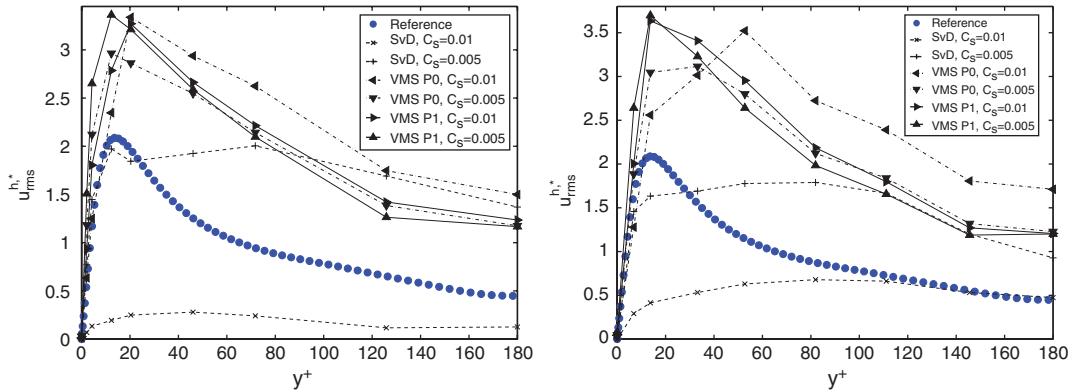
Figure 5. Simulations on the grids with an initial subdivision in y-direction into two layers, level 2, $u_{\mathrm{rms}}^{h,*}$, Grid 0 (left) and Grid 1 (right).
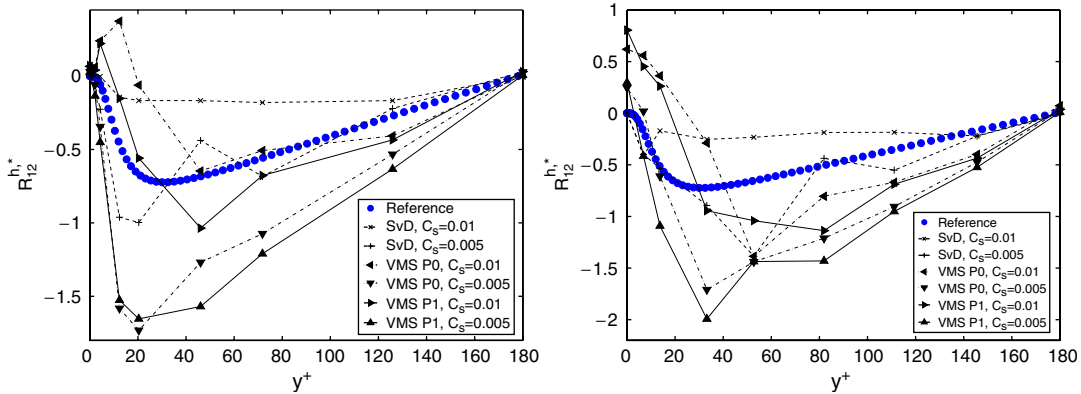

Figure 6. Simulations on the grids with an initial subdivision in y-direction into two layers, level 2, $\mathbb{R}_{12}^{h,*}$, Grid 0 (left) and Grid 1 (right).

The computed off-diagonal Reynolds stresses $\mathbb{R}_{12}^{h,*}$ are presented in Figure 6. In particular for Grid 1, the influence of the model $\mathbb{A}^h$ in computing the Reynolds stress at the wall for the VMS methods can be seen. Again, the VMS methods overpredict the absolute values quite a lot. A correct form of the curve is obtained only on Grid 0 for all methods with $C_s = 0.005$ (also the SvD method). The coarse near wall resolution of Grid 1 leads to peaks which are too far away from the wall.

Note that in comparable simulations (second order FVMs) from [21, 22] on a much finer grid ($32^3 = 32\,768$ grid cells), the second order statistics (turbulent kinetic energy) also show rather large differences to the reference curve. Thus, the use of second order spatial discretizations, which have much lower order than, for instance, spectral methods, might be an important reason for the considerable differences.
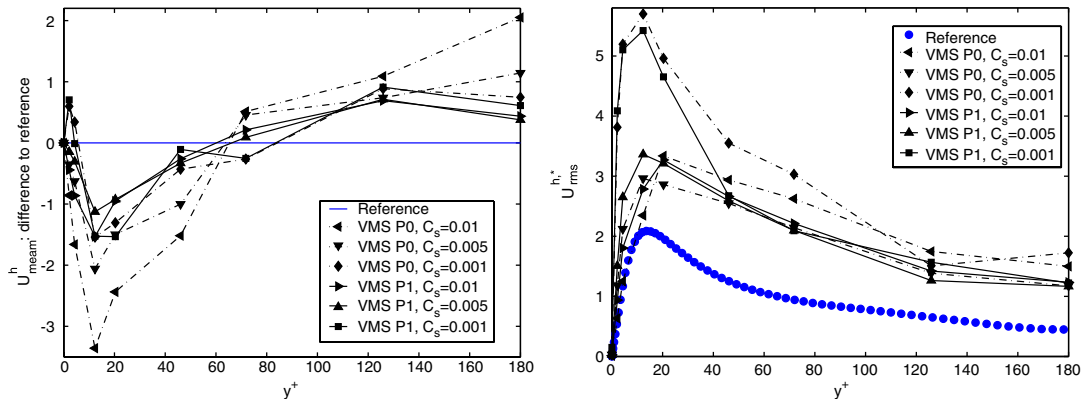
Figure 7. Simulations on the grids with an initial subdivision in y-direction into two layers, level 2, parameter study for the VMS methods, Grid 0, difference to the mean velocity profile (left), $u_{\mathrm{rms}}^{h,*}$ (right).

A parameter study for C_s in the VMS methods reveals that the results are best for $C_s = 0.005$, Figure 7. The choice of C_s has a greater impact on the results of VMS P0 than on the results of VMS P1. The great impact of C_s in the SvD method can be observed already in Figures 3–6.

Concerning the two distributions of the grid points in y-direction, the results on Grid 0 are in general better. This can be observed in particular for the second order statistics in Figures 5 and 6.

In summary, much better results are obtained on these very coarse grids with the VMS methods (VMS P0, $C_s = 0.005$; VMS P1, $C_s \in \{0.005, 0.01\}$) than with the SvD method. The mean stream-wise velocities are predicted quite well and the curves for the second order statistics are predicted qualitatively correctly (the off-diagonal Reynolds stress only Grid 0). However, the (absolute) values of the second order statistics are considerably overpredicted.

3.4. Simulations on grids with an initial subdivision into four layers

The results on the finer grids, which possess four mesh cell layers in y-direction on level 0, $l0 = 4$, and which are refined twice, are presented in Figures 8–12.

The SvD method with $C_s = 0.01$ gives poor results. Even the streamwise mean velocity profile is very badly captured. Concerning the VMS methods, the mean velocity profiles with $C_s = 0.01$ are somewhat better on both grids than with $C_s = 0.005$, see also Figure 11. The differences to the reference profile on Grid 1 are slightly smaller than on Grid 0.

The values for the rms turbulent intensities $u_{\mathrm{rms}}^{h,*}$ are too large for the VMS methods, Figure 9. These methods give better results with $C_s = 0.01$ than with $C_s = 0.005$. The SvD method with $C_s = 0.005$ computes similar results to the VMS methods. The evaluation of the results for $v_{\mathrm{rms}}^{h,*}$ and $w_{\mathrm{rms}}^{h,*}$ (not shown here) is quite similar.

Similar observations as for $u_{\mathrm{rms}}^{h,*}$ can be made for $\mathbb{R}_{12}^{h,*}$, Figure 10. The computed (absolute) values of the VMS methods are too large. Again, better results are obtained with $C_s = 0.01$. The SvD method with $C_s = 0.005$ behaves similarly to VMS P0 with $C_s = 0.01$.

A parameter study for the turbulence models, Figures 11 and 12, shows that choosing even smaller values than 0.005 worsens the results. However, the qualitative form of the curves for the VMS methods is correct for all parameters. This is in contrast to the SvD method with
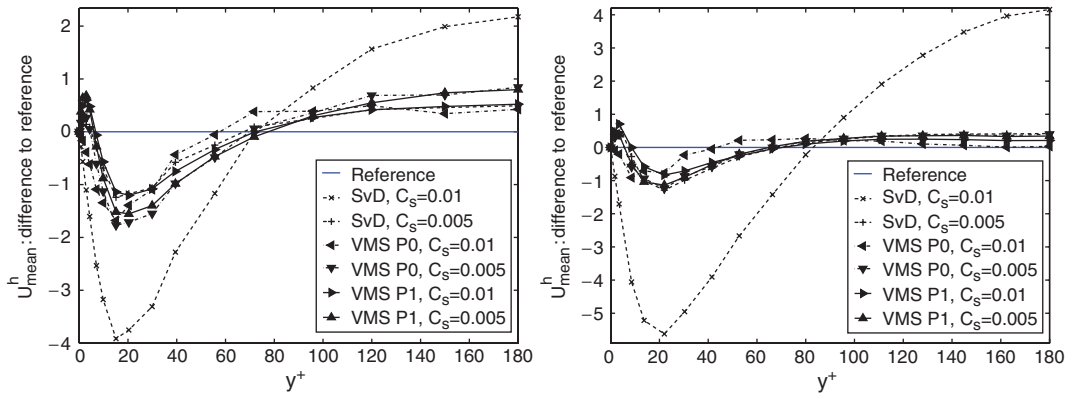
Figure 8. Simulations on the grids with an initial subdivision in y-direction into four layers, level 2, differences to the reference mean velocity profile, Grid 0 (left) and Grid 1 (right).
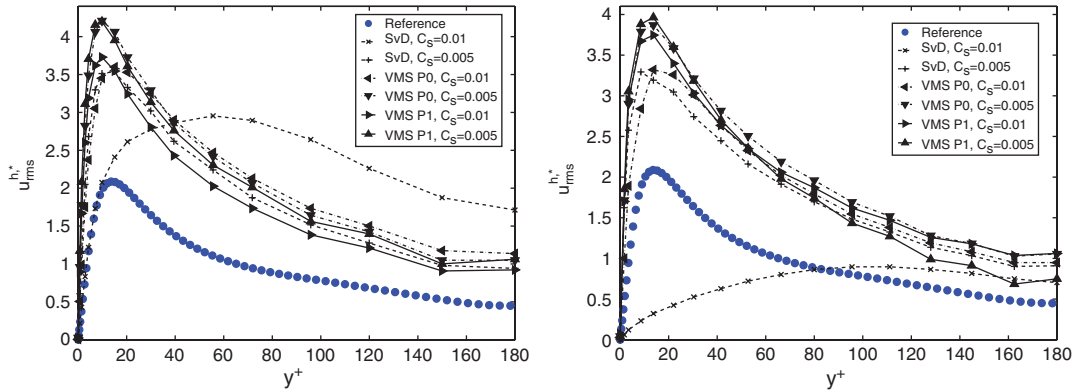

Figure 9. Simulations on the grids with an initial subdivision in y-direction into four layers, level 2, $u_{\mathrm{rms}}^{h,*}$, Grid 0 (left) and Grid 1 (right).

$C_s = 0.01$. It can be clearly observed that the choice of the parameter C_s has a much smaller influence in the VMS methods than in the SvD method. This reflects the philosophy of VMS methods—to apply a turbulence model only to scales where it is necessary and not to all scales. Thus, a variation of the parameters will affect much fewer scales directly and hence change the solution less.

Altogether, VMS P0 and VMS P1 with $C_s = 0.01$ and SvD with $C_s = 0.005$ give the best results in our numerical studies with an initial subdivision into four layers. The results of VMS P0 and VMS P1 with $C_s = 0.005$ are slightly worse whereas SvD with $C_s = 0.01$ gives completely wrong results. The results on Grid 1 are slightly better than on Grid 0.

3.5. Computational costs

The computing times of a number of simulations are given in Table II. A preconditioned flexible GMRES method with a multiple discretization multi-level preconditioner was used as solver, see
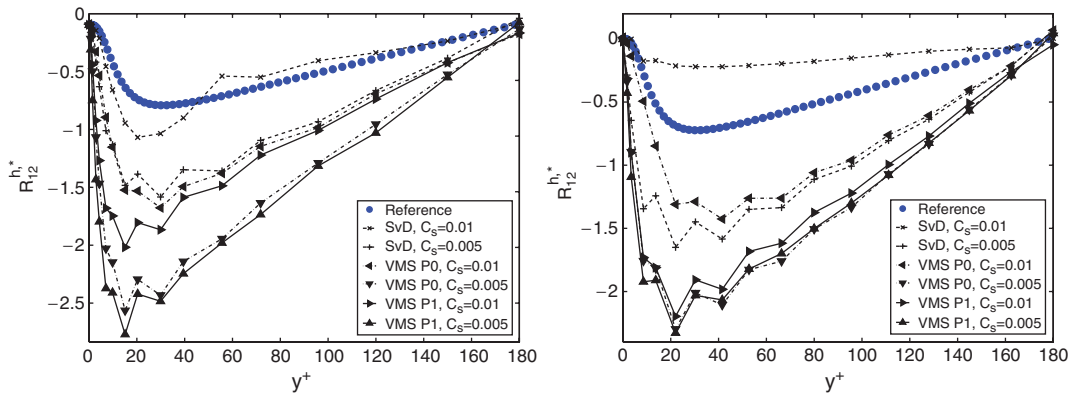
Figure 10. Simulations on the grids with an initial subdivision in y-direction into four layers, level 2, $\mathbb{R}_{12}^{h,*}$, Grid 0 (left) and Grid 1 (right).
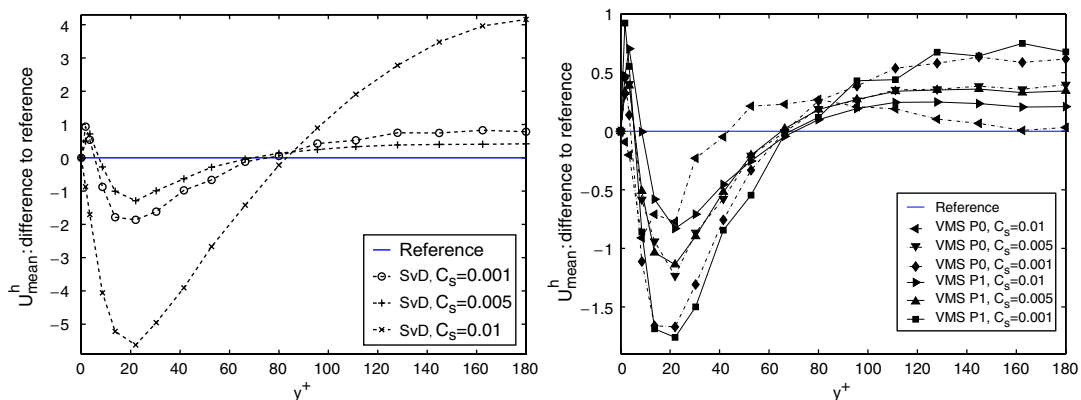

Figure 11. Simulations on the grids with an initial subdivision in y-direction into four layers, level 2, Grid 1, difference to the mean velocity profile, SvD (left), VMS methods (right).

[31, 35] for details. Roughly two-third of the computing time was spend for solving the non-linear systems and approximately one-third for assembling the matrices. The absolute computing times depend on the computer and the stopping criteria for the iterations. We would like to concentrate the evaluation on the comparison of the different methods and grids.

It can be seen that SvD was always the fastest method. The computations with VMS P0 were somewhat slower and the computations with VMS P1 took again somewhat more time. This corresponds to the observations in [27]. The computing times of VMS P0 were 7–33% longer than of SvD, however, the results are sometimes considerably better. We do not report computing times with $l0 = 4$, $C_s = 0.01$, since the results obtained with SvD were so different to the other results that a comparison of the computing times is meaningless.

Concerning the two grids, the computations on Grid 1 were in general faster. The reason is that the mesh cells close to the boundary possess a much higher aspect ratio on Grid 0 and our solver
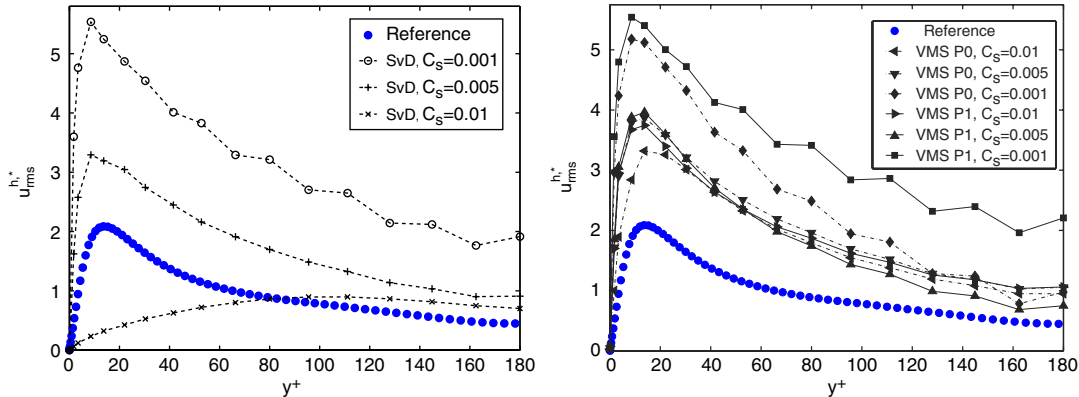
Figure 12. Simulations on the grids with an initial subdivision in y-direction into four layers, level 2, Grid 1, $u_{\text{rms}}^{h,*}$, SvD (left), VMS methods (right).

Table II. Computing times in seconds, in parentheses: percentage to computing time with SvD.

Parameters	SvD	VMS P0	VMS P1
$l0 = 2$, $C_s = 0.005$, Grid 0	166 698 (100)	221 995 (133)	230 680 (138)
$l0 = 2$, $C_s = 0.01$, Grid 1	128 112 (100)	144 559 (112)	156 352 (122)
$l0 = 4$, $C_s = 0.005$, Grid 0	576 729 (100)	732 632 (127)	934 427 (162)
$l0 = 4$, $C_s = 0.005$, Grid 1	557 518 (100)	597 509 (107)	643 438 (115)

looses some efficiency on grids with high aspect ratios. Doubling the initial subdivision of the domain from $l0 = 2$ to $l0 = 4$, which roughly doubles the number of d.o.f., leads to an increase in the computing times with a factor 3–4. However, also here has to be noted that the results for $l0 = 2$ and 4 are rather different since on the grids obtained with $l0 = 4$ more details of the flow field are simulated. This of course requires additional computational efforts.

Altogether, the better results of the VMS methods need somewhat higher computational costs. The reduction of these costs is an important topic for future research.

4. GALERKIN FINITE ELEMENT METHOD ON FINER GRIDS

This section studies the question of whether the use of turbulence models is still necessary for grids finer than those used in Section 3. It will be shown that refining those grids once, it is possible to apply even the Galerkin finite element method for the simulation of the turbulent channel flow at $Re_\tau = 180$. That means, no additional stabilization or modelling terms are used. Note that this property is studied in the present paper for the Q_2/P_1^{disc} finite element. Other finite element methods might need different refinement levels for the Galerkin method to be applicable. The usage of the Galerkin finite element method on a rather coarse mesh can be interpreted as an underresolved DNS or as a so-called MILES method. In a MILES method, the numerical diffusion takes the role of a turbulence model.
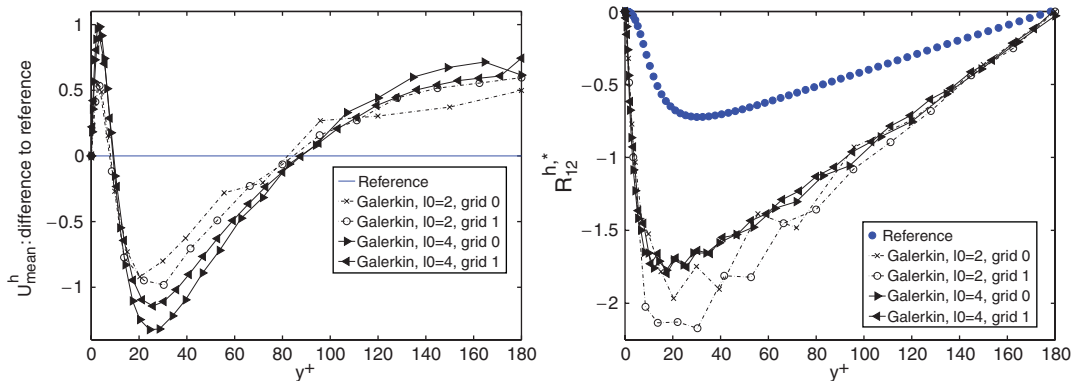
Figure 13. Galerkin finite element method on level 3, difference to the reference mean velocity profile (left) and $\mathbb{R}_{12}^{h,*}$ (right).
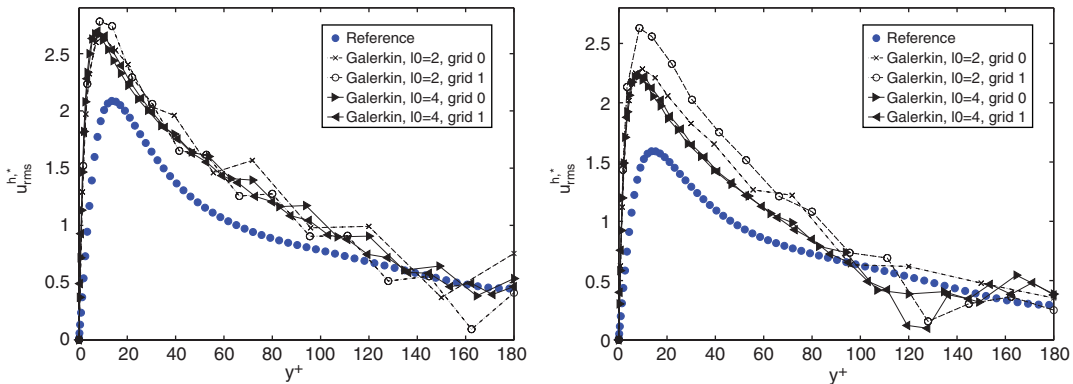

Figure 14. Galerkin finite element method on level 3, $u_{\mathrm{rms}}^{h,*}$ (left) and $v_{\mathrm{rms}}^{h,*}$ (right).

The results on the different grids are presented in Figures 13 and 14. The corresponding numbers of d.o.f. on level 3 are given in Table I. Concerning the mean velocity profile, the curves lie almost on top of each other such that we present only the differences to the reference profile. These differences are somewhat smaller than for the simulations with turbulence models on level 2. Using an initial subdivision into two layers, $l0 = 2$, leads close to the boundary, $y^+ \leqslant 5$ and in $y^+ \in [20, 40]$ to slightly smaller differences than using an initial subdivision into four layers, $l0 = 4$. The results for the Reynolds stress $\mathbb{R}_{12}^{h,*}$ are still quite far away from the reference curve. On the coarser grids, $l0 = 2$, the results are somewhat oscillatory. The rms turbulence intensities $u_{\mathrm{rms}}^{h,*}$ and $v_{\mathrm{rms}}^{h,*}$ are presented in Figure 14. The curves are closer to the reference curves than for the simulations with the turbulence models on level 2. Some oscillations can be observed towards the centre of the channel, in particular for the computations on Grid 1. The results obtained on Grid 0 are altogether slightly better.

In summary, the results for the mean velocity profile are satisfactory. The results for the second order statistics are not so good. However, one should keep in mind that on the one hand the grids are

still rather coarse. On the other hand, comparable simulations (second order spatial discretization) in [21, 22] show also rather large differences to the reference curves for second order statistics (turbulent kinetic energy).

5. SUMMARY

Simulations of turbulent channel flows at $Re_\tau = 180$ using projection-based finite element VMS methods and inf–sup stable, second/first order finite elements for the velocity/pressure were presented in this paper. The results obtained with projection-based VMS methods are compared to the Smagorinsky LES model with van Driest damping. The simulations were performed on very coarse meshes. The projection-based VMS methods gave in general good approximations of the mean velocity profile and good qualitative approximations of second order statistics. Quantitatively, the (absolute) values for the second order statistics are in general overpredicted. It could clearly be observed that the VMS methods are less sensitive to the choice of the parameter in the eddy viscosity model than the Smagorinsky LES with van Driest damping. It was demonstrated that refining the coarse grids once removes the need of using a turbulence model.

Further studies will be performed for turbulent channel flows at higher Reynolds numbers which will include also other approaches of VMS methods for finite element discretizations.

REFERENCES

1. Pope SB. *Turbulent Flows*. Cambridge University Press: Cambridge, 2000.
2. Sagaut P. *Large Eddy Simulation for Incompressible Flows* (3rd edn). Springer: Berlin, Heidelberg, New York, 2006.
3. John V. *Large Eddy Simulation of Turbulent Incompressible Flows. Analytical and Numerical Results for a Class of LES Models*. Lecture Notes in Computational Science and Engineering, vol. 34. Springer: Berlin, Heidelberg, New York, 2004.
4. Berselli LC, Iliescu T, Layton WJ. *Mathematics of Large Eddy Simulation of Turbulent Flows*. Springer: Berlin, 2006.
5. Smagorinsky J. General circulation experiments with the primitive equations: I. The basis equations. *Monthly Weather Review* 1963; **91**:99–164.
6. Germano M, Piomelli U, Moin P, Cabot W. A dynamic subgrid-scale eddy viscosity model. *Physics of Fluids A* 1991; **3**:1760–1765.
7. Lilly DK. A proposed modification of the Germano subgrid-scale closure method. *Physics of Fluids A* 1992; **4**:633–635.
8. Hughes TJR. Multiscale phenomena: Green's functions, the Dirichlet-to-Neumann formulation, subgrid-scale models, bubbles and the origin of stabilized methods. *Computer Methods in Applied Mechanics and Engineering* 1995; **127**:387–401.
9. Guermond J-L. Stabilization of Galerkin approximations of transport equations by subgrid modeling. *M2AN* 1999; **33**:1293–1316.
10. Hughes TJ, Mazzei L, Jansen KE. Large eddy simulation and the variational multiscale method. *Computing and Visualization in Science* 2000; **3**:47–59.
11. Collis SS. Monitoring unresolved scales in multiscale turbulence modeling. *Physics of Fluids* 2001; **13**:1800–1806.

12. Gravemeier V. The variational multiscale method for laminar and turbulent flow. *Archives of Computational Methods in Engineering* 2006; **13**:249–324.
13. John V. On large eddy simulation and variational multiscale methods in the numerical simulation of turbulent incompressible flows. *Applications of Mathematics* 2006; **51**:321–353.
14. Hughes TJR, Mazzei L, Oberai AA, Wray AA. The multiscale formulation of large eddy simulation: decay of homogeneous isotropic turbulence. *Physics of Fluids* 2001; **13**:505–512.
15. Hughes TJR, Oberai AA, Mazzei L. Large eddy simulation of turbulent channel flows by the variational multiscale method. *Physics of Fluids* 2001; **13**:1784–1799.
16. Oberai AA, Hughes TJR. The variational formulation of LES: channel flow at $Re_\tau = 590$. *AIAA Paper 2002-1056*, 2002.
17. Holmen J, Hughes JTR, Oberai AA, Wells GN. Sensitivity of the scale partition for variational multiscale large-eddy simulation of channel flow. *Physics of Fluids* 2004; **16**:824–827.
18. Ramakrishnan S, Collis SS. Turbulence control simulation using the variational multiscale method. *AIAA Journal* 2004; **42**:745–753.
19. Ramakrishnan S, Collis SS. Multiscale modeling for turbulence simulation in complex geometries. *AIAA Paper 2004-0241*, 2004.
20. Collis SS, Ramakrishnan S. The local variational multiscale method. *Third MIT Conference on Computational Fluid and Solid Dynamics*, Cambridge, MA, 2005.
21. Gravemeier V. A consistent dynamic localization model for large eddy simulation of turbulent flows based on a variational formulation. *Journal of Computational Physics* 2006; **218**:677–701.
22. Gravemeier V. Scale-separating operators for variational multiscale large eddy simulation of turbulent flows. *Journal of Computational Physics* 2006; **212**:400–435.
23. Calo VM. Residual-based multiscale turbulence modeling: finite volume simulations of bypass transition. *Ph.D. Thesis*, Department of Civil and Environmental Engineering, Stanford University, 2004.
24. Farhat C, Rajasekharan A, Koobus B. A dynamic variational multiscale method for large eddy simulations on unstructured meshes. *Computer Methods in Applied Mechanics and Engineering* 2006; **195**:1667–1691.
25. Gravemeier V, Wall WA, Ramm E. A three-level finite element method for the instationary incompressible Navier–Stokes equation. *Computer Methods in Applied Mechanics and Engineering* 2004; **193**:1323–1366.
26. Gravemeier V, Wall WA, Ramm E. Large eddy simulation of turbulent incompressible flows by a three-level finite element method. *International Journal for Numerical Methods in Fluids* 2005; **48**:1067–1099.
27. John V, Kaya S. A finite element variational multiscale method for the Navier–Stokes equations. *SIAM Journal on Scientific Computing* 2005; **26**:1485–1503.
28. John V, Kaya S, Layton W. A two-level variational multiscale method for convection-dominated convection–diffusion equations. *Computer Methods in Applied Mechanics and Engineering* 2006; **195**:4594–4603.
29. John V, Tambulea A. On finite element variational multiscale methods for incompressible turbulent flows. *Proceedings of ECCOMAS CFD 2006* (on CD ROM), 2006. ISBN: 90-9020970-0.
30. Jansen KE, Tejada-Martinez AE. An evaluation of the variational multiscale model for large-eddy simulation while using a hierarchical basis. *AIAA Paper 2002-0283*, 2002.
31. John V. Higher order finite element methods and multigrid solvers in a benchmark problem for the 3D Navier–Stokes equations. *International Journal for Numerical Methods in Fluids* 2002; **40**:775–798.
32. John V. Reference values for drag and lift of a two-dimensional time dependent flow around a cylinder. *International Journal for Numerical Methods in Fluids* 2004; **44**:777–788.
33. Moser DR, Kim J, Mansour NN. Direct numerical simulation of turbulent channel flow up to $Re_\tau = 590$. *Physics of Fluids* 1999; **11**:943–945.
34. Turek S. *Efficient Solvers for Incompressible Flow Problems*: *An Algorithmic and Computational Approach*. Lecture Notes in Computational Science and Engineering, vol. 6. Springer: Berlin, 1999.
35. John V. On the efficiency of linearization schemes and coupled multigrid methods in the simulation of a 3d flow around a cylinder. *International Journal for Numerical Methods in Fluids* 2006; **50**:845–862.
36. John V, Matthies G, Rang J. A comparison of time-discretization/linearization approaches for the time-dependent incompressible Navier–Stokes equations. *Computer Methods in Applied Mechanics and Engineering* 2006; **195**:5995–6010.
37. Gresho PM, Sani RL. *Incompressible Flow and the Finite Element Method*. Wiley: Chichester, 2000.
38. John V, Matthies G. Higher order finite element discretizations in a benchmark problem for incompressible flows. *International Journal for Numerical Methods in Fluids* 2001; **37**:885–903.
39. Choi H, Moin P. Effects of the computational time step on numerical solutions of turbulent flow. *Journal of Computational Physics* 1994; **113**:1–4.

40. Morinishi Y, Vasilyev OV. A recommended modification to the dynamic two-parameter mixed subgrid scale model for large eddy simulation of wall bounded turbulent flow. *Physics of Fluids* 2001; **13**:3400–3410.
41. Winckelmans GS, Jeanmart H, Carati D. On the comparison of turbulent intensities from large-eddy simulation with those from experiment or direct numerical simulation. *Physics of Fluids* 2002; **14**:1809–1811.
42. Iliescu T, Fischer P. Large eddy simulation of turbulent channel flows by the rational LES model. *Physics of Fluids* 2003; **15**:3036–3047.
43. John V, Matthies G. MooNMD—a program package based on mapped finite element methods. *Computing and Visualization in Science* 2004; **6**:163–170.
44. van Driest ER. On turbulent flow near a wall. *Journal of the Aerospace Sciences* 1956; **23**:1007–1011.
45. Hughes TJR, Wells GN, Wray AA. Energy transfer and spectral eddy viscosity in large-eddy simulations of homogeneous isotropic turbulence: comparison of dynamic Smagorinsky and multiscale models over a range of discretizations. *Physics of Fluids* 2004; **16**:4044–4052.
46. Gravemeier V. Variational multiscale large eddy simulation of turbulent flow in a diffuser. *Computational Mechanics* 2007; **39**:477–495.
47. Deardoff JW. A numerical study of 3-d turbulent channel flow at large Reynolds numbers. *Journal of Fluid Mechanics* 1970; **41**:453–480.
48. Meyers J, Sagaut P, Guerts BJ. Optimal model parameters for multi-objective large-eddy simulations. *Physics of Fluids* 2006; **18**:095103.